Geological and Stratigraphic Relationships between Slump Deposits and Stacked Delta Deposits in the Melas Chasma Rift Margin, Valles Marineris

M. L. Schlaak[1], G. P. Roberts[2]

[1]Department of Physics and Astronomy, University College London, Gower Street, London WC1E 6BT, UK

[2]Department of Earth and Planetary Sciences, Birkbeck, University of London, Malet St., London, WC1E7HX

Corresponding author: Marius Schlaak (Marius.Schlaak@tum.de)

Key Points:

- Stacked delta deposits located on the hangingwall of normal fault inside Melas Chasma on Mars are mapped using sequence stratigraphy.
- The Kerinitis delta is used as a terrestrial analogue example for the structures, such as clinoforms, observed in Melas Chasma.
- Compared terrestrial and Martian slip-rates give a timescale of 1.25 to 15 million years for a water body existing on the Martian surface.

Abstract

In order to assess the sedimentological and stratigraphic history of the Melas Chasma rift basin, Mars, and investigate the possibility of past bodies of water, we have mapped Hesperian stacked sedimentary deposits containing what appear to be 10^2 m scale topsets, clinoforms, toesets and olistoliths located on the immediate hangingwall of a normal fault, and correlated these with folded and slumped units on the basin floor. The vertical extent of clinoforms suggest deposition in bodies of water that were tens to hundreds of metres deep associated with gravity-driven mass-movement of sediment to the basin floor. We correlated the basin margin deposits with basin-floor deposits by mapping unconformities, which define four depositional sequences. Using the principles of sequence stratigraphy in rifts, developed for terrestrial analogues in the Gulf of Corinth, Greece, we infer the history of the Melas Chasma deposits. Results suggest that water-high-stand delta deposits became stacked across unconformities in a basin undergoing active hangingwall subsidence. Assuming slip-rates on the basin-bounding normal fault similar to that found on other terrestrial and Martian faults, we infer timescales of ~1.25 to 15 million years for the sedimentation and water body. We discuss our findings in terms of a possible connection to the putative paleo-ocean on the Martian northern hemisphere.

Plain Language Summary

This work suggests that the sediments in Melas Chasma, a large valley on Mars, have the same characteristics as sediments on Earth that developed in a comparable geologic settings and are therefore of similar origin. This conclusion allows a comparison of the examples such as the Gulf of Corinth, Greece, and the Dead Sea. Sedimentation in Melas Chasma was controlled by subsidence, evidenced by distinct stacked sediment packages tens of hundreds of metres thick. Of special interest for establishing a timescale are the rates of the tectonic lowering, which are well known for examples on Earth and also estimated for some regions on Mars. Together with the thickness of the sediments of more than 1500 metres and a range of possible rates for the subsidence the timescale of 1.25 and 15 million years is estimated. Moreover, the sedimentary structures suggest a long-lived water body that was several tens to hundreds of metres deep. The novel finding of this work is the identification of stacked sediment sequences separated by major unconformities, not previously reported from Mars; this supports the idea that the Martian climate in the Hesperian age allowed a large lake or even ocean to exist for millions of years.

1 Introduction

An ongoing debate concerns the past existence of large water bodies on Mars. To date studies have identified a number of possible examples of sedimentary deposits and landforms that may indicate extensive water bodies that persisted for as long as millions of years, including sediments infilling pre-existing craters, or possible palaeo-shorelines from, for example, a possible northern hemisphere ocean (Barker & Bhattacharya, 2017; Parker, Gorsline, Saunders, Pieri, & Schneeberger, 1993; Parker, Saunders, & Schneeberger, 1989). However, a common feature of these is that observations have been linked to a single depositional phase, and, in general, we lack examples where sediments can be placed in the context of long-lived sedimentary basins. On Earth, sedimentary basin deposits are typified by multiple depositional phases, with sedimentary sequences separated by syn-depositional unconformities (Backert, Ford, & Malartre, 2010; Ford et al., 2007). The unconformities are produced by water level fluctuations associated with both absolute sea-level changes produced by climate change, and relative sea-level changes produced by local uplift/subsidence associated with active geological structures such as faults, folds and broad areas of vertical motion associated with thermal subsidence (Dart, Collier, Gawthorpe, Keller, & Nichols, 1994; van Wagoner et al., 1988). Observations of syn-depositional unconformities separating sedimentary sequences that can be placed into the context of sedimentary basin evolution, and also spatial variations in synchronous sedimentary processes produced by changes in vertical motion across basins, can be used to derive a better understanding of the timescales of sedimentary processes, but we lack such information from Mars. This paper provides an example from the Valles Marineris rift basin where we suggest that it is possible to link observations of separate sedimentary sequences, defined by intervening unconformities, with spatial variation in sedimentary processes such as shallow water fan/delta formation and deeper water sedimentary slumping and mass movement, that we can link to vertical motion across the normal faults that controlled the basin.

For example, studies on Mars, have reconstructed paleo-climate conditions by examining impact craters and the global hydrogen distribution (Feldman et al., 2004). Many sites suggest a history of alluvial, and lacustrine/marine processes e.g. the delta deposits in the Eberswalde Crater (Malin & Edgett, 2003; Pondrelli et al., 2008), the alluvial fans in Valles Marineris (J. Metz, Grotzinger, Okubo, & Milliken, 2010) and cross-bedding in the Gale Crater (Anderson & Bell III, 2010; Grotzinger et al., 2015; Laetitia Le Deit et al., 2013). Furthermore, a supporting

argument for large water bodies is the Martian topography, as evidenced by the dichotomy between the southern and northern hemispheres. The existence of paleo-shorelines along the topographical boundary have been suggested to indicate a paleo-ocean in the northern hemisphere (Parker et al., 1989). Additional to the shorelines, sedimentary fans and inverted fluvial channels are observed along the Martian dichotomy border in Hypanis Valles indicating an ancient waterbody covering at least Chryse Planitia (Fawdon et al., 2018). On a smaller scale, the topography of old degraded Noachian craters was investigated, suggesting that the morphologies originate from rainfall and surface runoff (Craddock & Howard, 2002; Forsberg-Taylor, Howard, & Craddock, 2004). Further examinations with spectral chemistry analyses discovered clay minerals and hydrated sulphates in Martian deposits (Bibring et al., 2006), while additional evidence for the existence of water ice in the sub-surface is provided hydrogen maps (Feldman et al., 2004). Overall, there are significant indicators for the previous existence of large water bodies on Mars, but the length of time they lasted, and their association with sedimentary basins is a matter of debate. The described deposits are typically single sequences rather stacked sequences separated by major unconformities that typify terrestrial sedimentary basins, so the interpreted water depths and accommodation space are typically relatively shallow. So far, terrestrial sedimentation rates have been used to estimate the duration of lacustrine activity inside Gale Crater. These estimates vary between 100 a to a maximum of 10 ka with paleowater depths of tens of metres inferred by delta deposits (Grotzinger et al., 2015), and 1 ka to 10 Ma, inferred by the presence of thousands of laminae in thick fine-grained deposits (Stack et al., 2019).

The example we study is located in Melas Chasma, which is part of the rift system Valles Marineris (Fig. 1). The area of study is located on the south margin of Valles Marineris and shows stacked layered deposits merging into slumped units. Assuming the existence of normal faults along the margins of the rift valley, we attempt to map and correlate sediments and unconformities to establish both the water depths and timescales for the sedimentation, comparing the deposit thicknesses with possible slip-rates for the normal faults. Our interpretation of stacked delta deposits in such a tectonic setting have implications for Martian history and climate conditions.

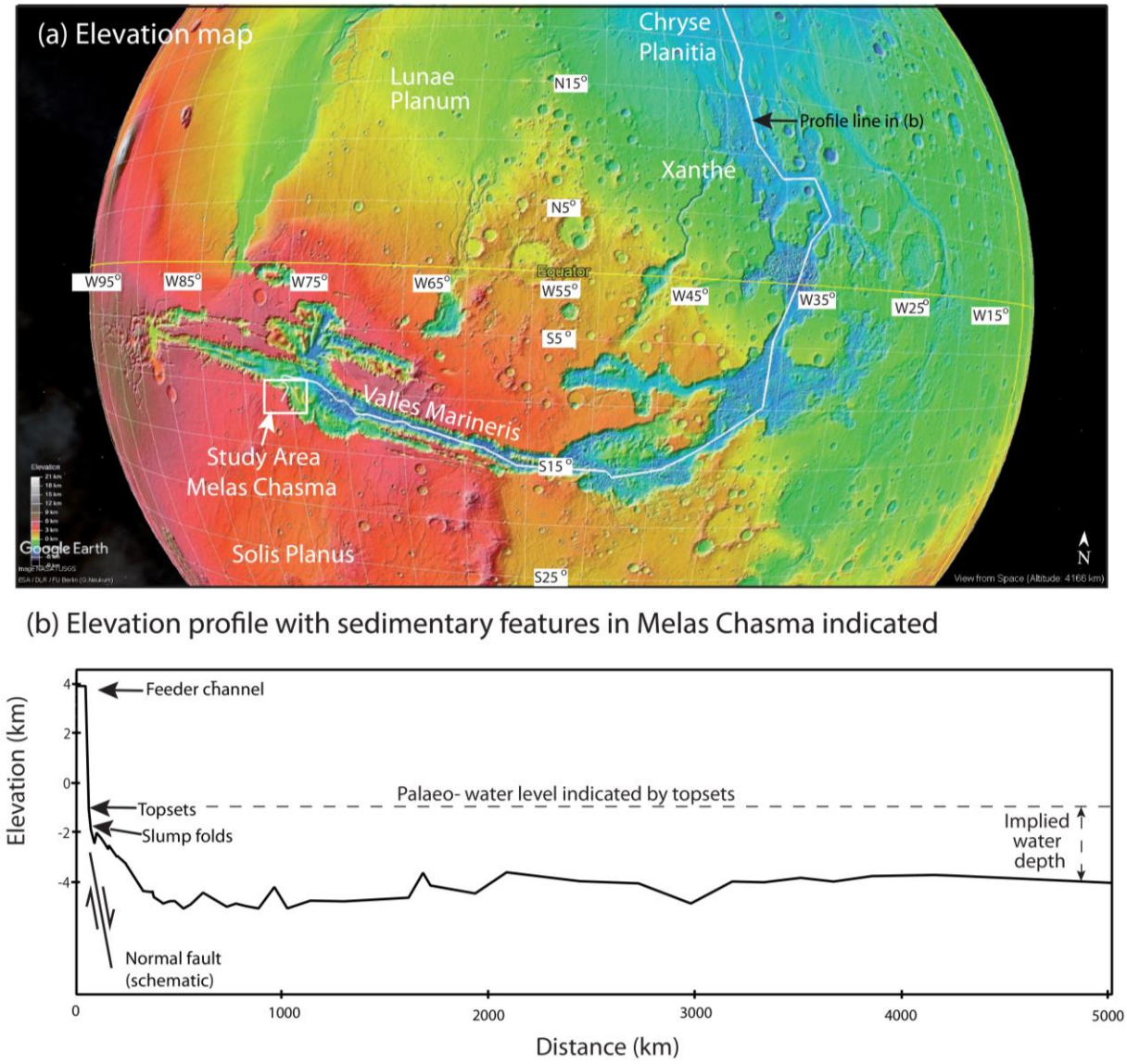

Figure 1: (a) Colourized terrain from (Credits: NASA/JPL/MSSS/Caltec Murray Lab/Esri) showing the area of study in Valles Marineris and topographic relations on the planet. (b) shows a elevation profile between the area of study and the northern lowlands with the sedimentary features in Melas Chasma indicated.

2 Geological Background to Melas Chasma

Valles Marineris is a 4000 km long canyon system, trending east-west, with Melas Chasma located in its centre (Witbeck, Tanaka, & Scott, 1991). It has a lowest elevation of ca. 5 km below the surrounding plateaus. By comparing terrestrial rift examples and image observation, the origin of the large canyon system has been linked to extensional stresses of the Tharsis rise in combination with passive rifting resulting into graben structures (Mège &

Masson, 1996). A detailed geomorphologic study identified faults showing a complex tectonic activity in the past of Melas Chasma (Peulvast & Masson, 1993), with horst and graben structures assumed to be buried underneath the sediments inside Melas Chasma (Mège & Masson, 1996).

Melas Chasma was not only shaped by tectonic activity. Further, there are features like clinoforms and channel levees (Dromart, Quantin, & Broucke, 2007), valley networks (Quantin, Allemand, Mangold, Dromart, & Delacourt, 2005), and sub-lacustrine fans (Joel Michael Davis, 2017; J. M. Metz et al., 2009) that indicate a water body or deep lake in the Melas Chasma. The more recent shape of Valles Marineris is controlled by faults, landslides, as well as wind erosion, and gullying (J. M. Davis et al., 2018; Lucchitta, 1979; Witbeck et al., 1991)

3 Materials and Methods

3.1 Satellite Data

In this work CTX and HiRISE images from the Mars Reconnaissance Orbiter (MRO) were used as background images for the mapping. The Context Camera (CTX) provides images with a resolution of ca. 6 m/pixel (Malin et al., 2007). The High-Resolution Imaging Science Experiment (HiRISE) images have a much higher resolution (0.25 to 1.3 m/pixel) but less coverage (McEwen et al., 2007). The High-Resolution Stereo Camera (HRSC) is part of the Mars Express ESA mission obtaining global topographic data with a horizontal resolution of 50 m and DTMs with locally horizontal resolutions up to 10 m and better (Gwinner et al., 2009). We use a global DTM from HRSC data blended with MOLA created by Fergason, Hare, and Laura (2018) to estimate dipping directions and sediment thickness.

Additional hyperspectral images are locally available from the Compact Reconnaissance Imaging Spectrometer for Mars (CRISM) onboard the MRO. CRISM provides a range from visible to near-infrared wavelengths (0.37 to 3.92 µm) (Murchie et al., 2007). The resolution of the data is ~200 m/pixel on a global scale and increases to ~20 m/pixel for selected areas. The mafic minerals can be detected on a global scale, whereas hydrated minerals as phyllosilicates and sulphates only occur on a regional scale (Pelkey et al., 2007).

3.2 Mapping Methods

A base map of the area of interest was produced by aligning the georeferenced satellite imagery in QGIS. During the geologic mapping, contacts between characteristic units have been traced. The units have been determined by a change in texture, colour, spectral properties, strike, and dip, as well as by unconformities. By correlating the different unconformities, it was possible to give the relative age relation between the units, based on the principles of sequence stratigraphy.

3.3 Sequence stratigraphy

As will be shown below, the existence of unconformities separating distinct sedimentary sequences in Melas Chasma allows us to use the principles of sequence stratigraphy to unravel the history of sedimentation and discuss its wider implications. Sequence stratigraphy provides a powerful tool to analyse time and rock relationships in a stratigraphic framework of genetically related repetitive strata often used in sediment stratigraphy (Backert et al., 2010; Bartov, Stein, Enzel, Agnon, & Reches, 2002; Dart et al., 1994; Gawthorpe, Fraser, & Collier, 1994).

Of particular interest to this study is the typical sequence stratigraphy of rift basins derived from studies on the Earth (Backert et al., 2010; Gawthorpe et al., 2017; Gawthorpe, Hardy, & Ritchie, 2003; Rohais, Eschard, & Guillocheau, 2008). In these examples, the typical deposits are basin-margin fan/deltas, which may be stacked vertically on top of each other, separated by unconformities, in the hangingwalls of normal faults, with down-dip deeper water deposits that are typically affected by mass movement down-slope to form slumped units and turbidites. A terrestrial example of this comes from the Gulf of Corinth, Greece, where Quaternary glacio-eustatic sea-level changes, and vertical motions associated with active normal faults, have produced extensive outcrops of stacked basin-margin delta deposits up-dip from basin floor mass-wasting deposits. Deltas can be recognized by their geometries and typical tripartite subdivision into topsets, foresets, also known as clinoforms, and bottomsets (also known as toesets), as first described by Gilbert (1885). The topsets are horizontal, relatively thin layers of coarse material fed by feeder channels that are typically alluvial to delta-top marginal marine/lacustrine. The recognition of foresets is aided by the observations that they diverge from horizontal topsets at a clearly defined shelf-edge break, dipping towards the basin with a 10°-25° angle. The foresets typically down-lap onto, or merge into, the basin floor deposits, with

basinward progression of the points of down-lap indicating foreset progradation. Progradation generally occurs if water level remains relatively constant and sediment supply continues to fill the available space for sedimentation between the basin floor and water level. The vertical extent of the foresets/clinoforms defines the water depth at the time of deposition, as defined by the vertical separation of the shelf-break and point of downlap. Foresets may also contain olistoliths, which are coherent blocks of pre-existing lithified sediment or bedrock, which have been mobilised and moved downslope into deeper water. Down-dip of the fan deltas, toesets and associated basinal deposits are commonly turbidites intercalated with horizons containing slump folds, debris flows typical of mass-wasting deposits. Details of these geometries and sediments from terrestrial examples are given in many papers, for example those by (Backert et al., 2010; Dart et al., 1994; Ford et al., 2007; Gawthorpe et al., 2003; Gawthorpe, Colella, & Prior, 1990; Gilbert, 1885), but, to date, we lack observations of them from Mars.

Once the sedimentary geometries described above have been identified, one can reconstruct the past events, such as vertical motions caused by local tectonics or more regional/global water-level fluctuations. This is achieved by dividing the deposits into depositional sequences and through study of their relative geometries and internal geometries. In terms of relative geometries, sequences can be superimposed horizontally or vertically depending on the relative sea-level changes, accommodation space and sediment supply, which are in turn controlled by position in the basin, such as footwall or hangingwall locations. For example, where subsidence rates are high relative to sedimentation rate, due to a position in the immediate hangingwall of an active normal fault, sequences consisting of delta deposits can be become stacked on top of each other, with toe-sets either down-lapping onto the previous lowstand unconformity (so-called Type 1 sequence boundary) developed on top of previous top-set deposits, or merging into thin basinal deposits that will be characterized by stacked distal deposits separated by unconformities lacking angular discordance (Dart et al., 1994; Gawthorpe et al., 2003; van Wagoner et al., 1988). Individual delta sequences can exhibit progradational internal geometries, where sediment supply is high relative to subsidence rate during relative sea-level highstand, but the geometric arrangement of subsequent deltas are typically stacked due to the high subsidence rates on the fault, exacerbated by times of lowstand when the sediment supply tends to drop due to forced regression of the coastline and incision of past coastlines and by-pass of sediment to positions that were formerly in deeper water. Each new delta re-occupies

up-dip positions during sea-level rise, forming above a flooding surface that is typically parallel in part to the former Type 1 sequence boundary (Fig. 2). Thus, the relative geometry of subsequent deltas is mainly controlled by the creation of accommodation space by local tectonic subsidence and sea-level rise, given sediment supply.

Melas Chasma is a rift basin, which is well known to contain layered deposits (Joel Michael Davis, 2017; Dromart et al., 2007; Liu & Catalano, 2016; J. M. Metz et al., 2009; Quantin et al., 2005a) containing kilometre-scale folds that resemble slumps (J. Metz et al., 2010), and has landforms that resemble drainage systems (Quantin et al., 2005a). Additional drainage systems could have been existent that would have transported water and sediments from the rift basin to the west and then the north into the relatively low topography of the northern hemisphere of Mars that has been suggested to have been, at times, a water-filled basin (Barker & Bhattacharya, 2017; Carr, 2003; Head et al., 1999; Parker et al., 1993).

Our new observations are that the layered deposits contain unconformities between packages of slumped deposits, and have not previously been mapped and reported in detail to reveal the relationships between these slump packages, or to correlate between basin floor slumps and basin margin deposits that lack slumps and appear to be thicker-bedded, massive deposits. Furthermore, we suggest that the up-dip, basin margin, massive deposits contain unconformities, and examples of clinoforms and olistoliths, whose relationships have not been previously mapped or correlated with the basin floor deposits. In this paper, we use concepts of sequence stratigraphy to study the deposits of Melas Chasma. We find that the deposits exhibit a strong resemblance to rift basin deposits on the Earth, comparing them with well-studied sequences in the Gulf of Corinth rift, Greece.

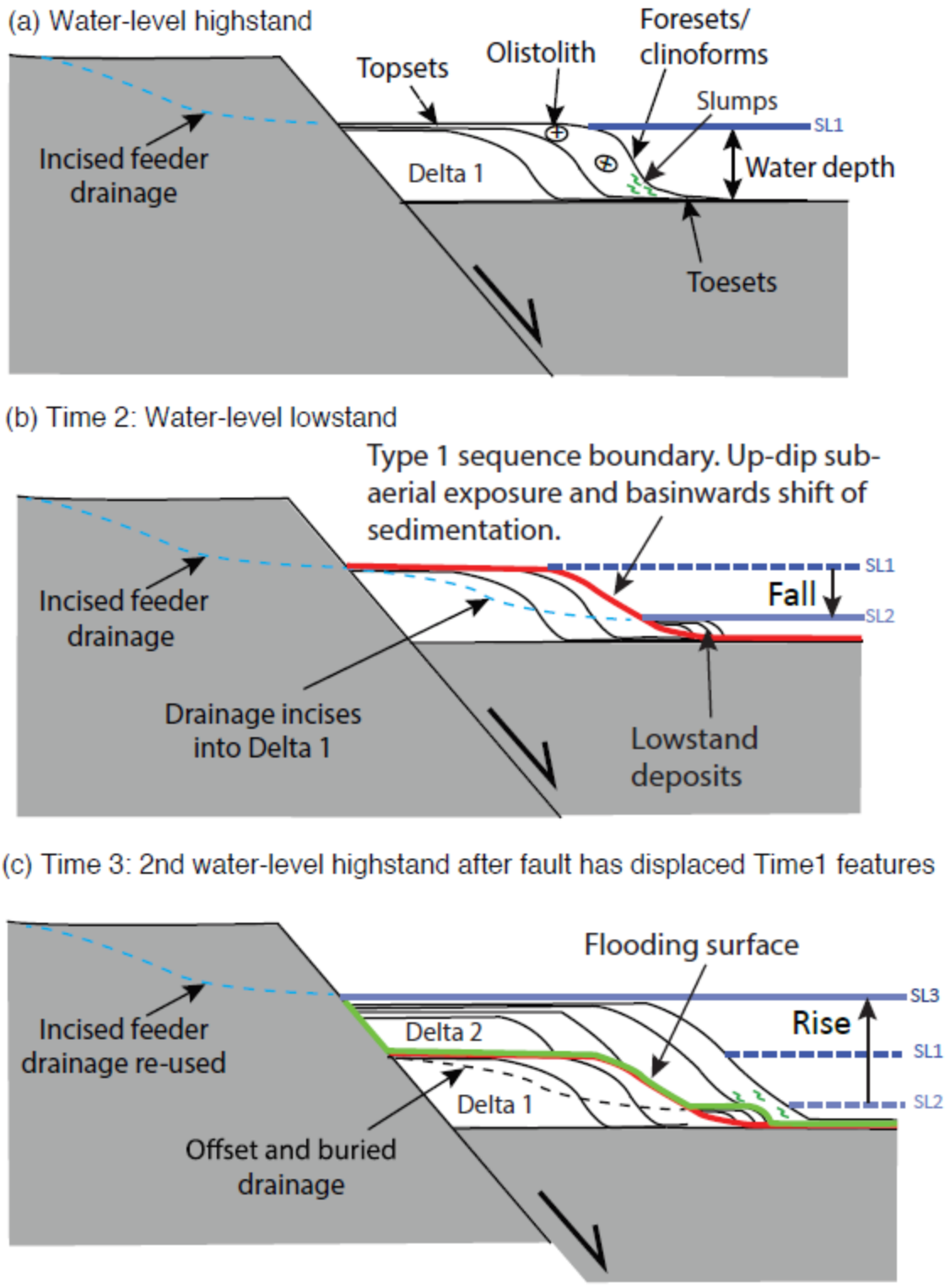

Figure 2: The schematic sketches show different form of depositions depending on water level falls of rises. (**a**) Relative highstand and delta forms. (**b**) shows Water-level fall and the formation of Type 1 sequence boundary and lowstand deposits. (**c**) Water-level rise. A flooding surface forms during transgression, such that water covers the

previous delta due to ongoing fault slip and subsidence. A new delta progrades over the flooding surface, after back-filling the lowstand drainage channel that incised into Delta 1, with slumps at the base of toe-sets. Delta 1 and Delta 2 are stacked on top of each other, separated by an unconformity that is a composite surface composed of a closely-spaced Type 1 exposure surface and superimposed flooding surface.

4 Results

4.1 Initial observations and overview of interpreted sedimentary features

The SW margin of Melas Chasma is characterised by a ~6 km deep valley containing layered deposits adjacent to an escarpment rising to the relatively flat plateau area of Solis Planum (Fig. 3). Initial observations of the SW margin of Melas Chasma, revealed that the highest elevation layered deposits display massive layers, dipping radial away from the margin, with units at lower elevations on the valley floor displaying interlayering of resistant and less resistant bands with complex folding (Figs. 3, 4, 5 and 6).

4.2 High elevation massive layers.

Closer examination revealed that the high elevation massive layers have relatively low dips of a few degrees, with layers almost coincident with topographic contours (Fig. 4a). However, subtle changes in dip and strike within these rocks define angular unconformities that can be followed across the whole mapping area (distances of 10-15 km) until they are covered by younger deposits at the margin. Beds between the unconformities appear to show a tripartite division (Fig. 4b). (1) Immediately above an unconformity, the layers are relatively thin with almost horizontal dips. The layers thin down downwards and terminate onto the underlying unconformities. This resembles the downlap geometry that characterises the toesets of terrestrial deltas. (2) Up dip of these interpreted toesets, the beds thicken and display dips up to at least 7^{o} in places, before thinning up-dip with reduced dip angles. The layers appear to be truncated by almost horizontal local unconformities that we have been unable to trace laterally for more than a few hundred metres (Fig. 4c). The layers also appear to dip radially away from the margin of Melas Chasma (Fig. 4b). These geometries resemble clinoforms that terminate up-dip into erosional truncation surfaces from terrestrial deltas. The clinoforms also contain examples of large blocks, up to 300 m across, with lithologies that differ from the surrounding material, with layering in the surrounding material terminating at the margins of blocks (Fig. 4d). These resemble olistoliths within the clinoforms reported from terrestrial deltas. (3) Above the local

unconformities that we interpret as erosional truncation surfaces, the layers are relatively-thin and shallowly dipping, parallel to the underlying erosional truncation surface. These resemble topsets overlying an erosional truncation surface from terrestrial deltas (Figs. 4b and c). Overall, our interpreted tripartite subdivision into toesets, clinoforms with olistoliths, and topsets suggests that these are Gilbert delta deposits. Furthermore, higher on the escarpment, we have identified what appear to be feeder channels for the Gilbert deltas (Fig. 5). Convex downward channel geometries are clear in the cliffs forming the escarpment edge, and the map traces of the feeder channels appear to be visible defined by subtle changes in the grayscale of CTX and THEMIS images.

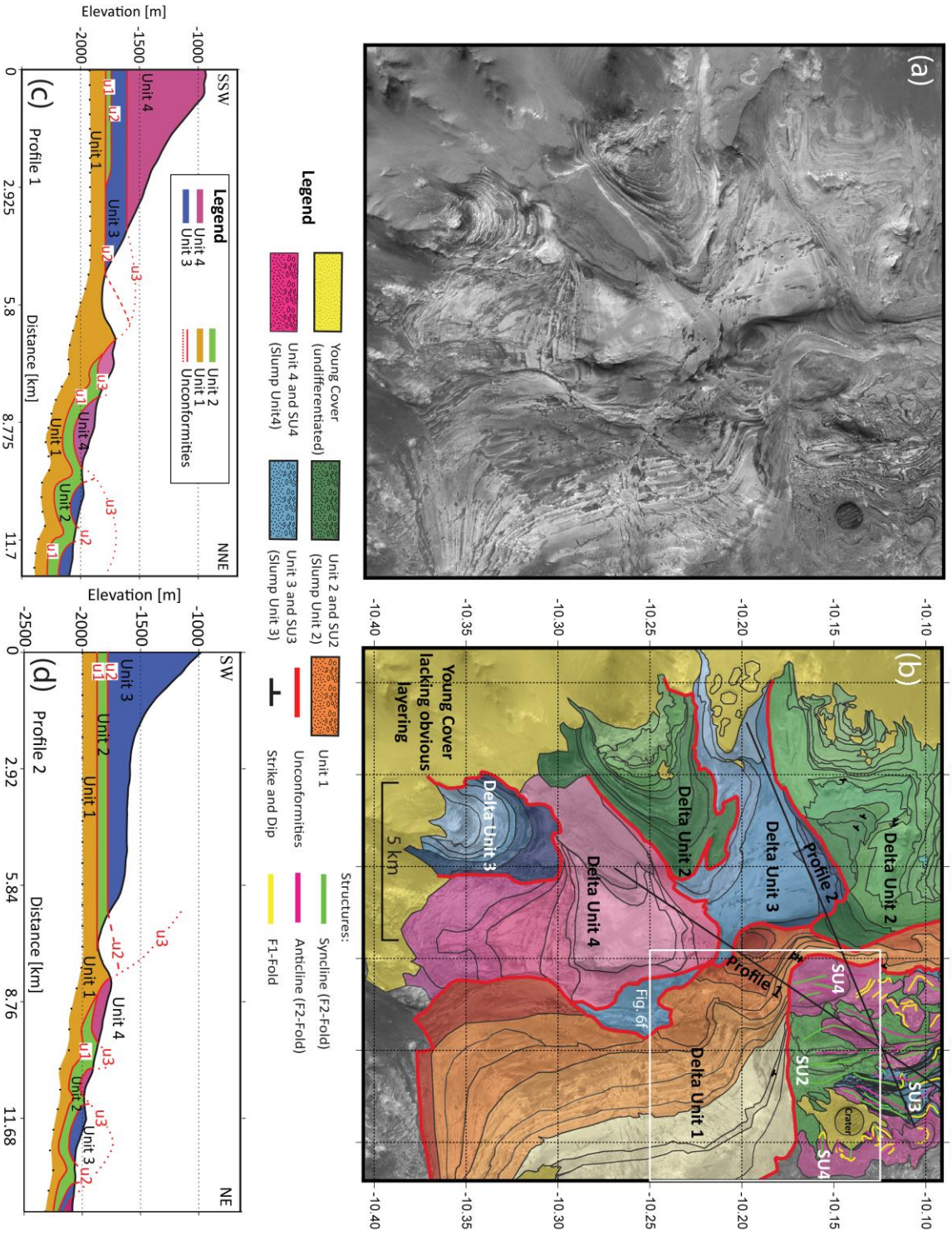
(a)
(b)
(c)
(d)
Delta Unit 2
Delta Unit 3
Delta Unit 4
Delta Unit 1
Young Cover lacking obvious layering
Profile 1
Profile 2
Fig. 6f
SU3
SU4
SU2
Crater
5 km
-10.10
-10.15
-10.20
-10.25
-10.30
-10.35
-10.40
-75.55
-75.50
-75.45
-75.40
-75.35
-75.30
Legend
Young Cover (undifferentiated)
Unit 2 and SU2 (Slump Unit 2)
Unit 4 and SU4 (Slump Unit4)
Unit 3 and SU3 (Slump Unit 3)
Unit 1
Unconformities
Strike and Dip
Structures:
Syncline (F2-Fold)
Anticline (F2-Fold)
F1-Fold
Elevation [m]
-1000
-1500
-2000
-2500
SSW
NNE
SW
NE
Unit 4
Unit 3
Unit 2
Unit 1
Unconformities
u1
u2
u3
Profile 1
Profile 2
Distance [km]
0
2.925
5.8
8.775
11.7
2.92
5.84
8.76
11.68

Figure 3: (**a**) Uninterpreted CTX imagery of the area of interest (**b**) The overview map of the area of interest. The sequences are located in the west, and the slumped are in the northeast. The unconformities are marked in red. The green and pink lines in the slumped area represent the folding axis of secondary deformation features. The yellow lines indicate primary deformation. Profile 1 is 12.6 km long, Profile 2 14 km, they intersect with several different deltaic and slumped units illustrating the stratigraphy.

We note that the Gilbert deltas we have identified are juxtaposed laterally next to each other in map view, and integration of topographic information show that deltas overlie each other and appear to be vertically stacked. We performed geological mapping of these units and unconformities that separate them in order to understand the stratigraphic relationships in the area.

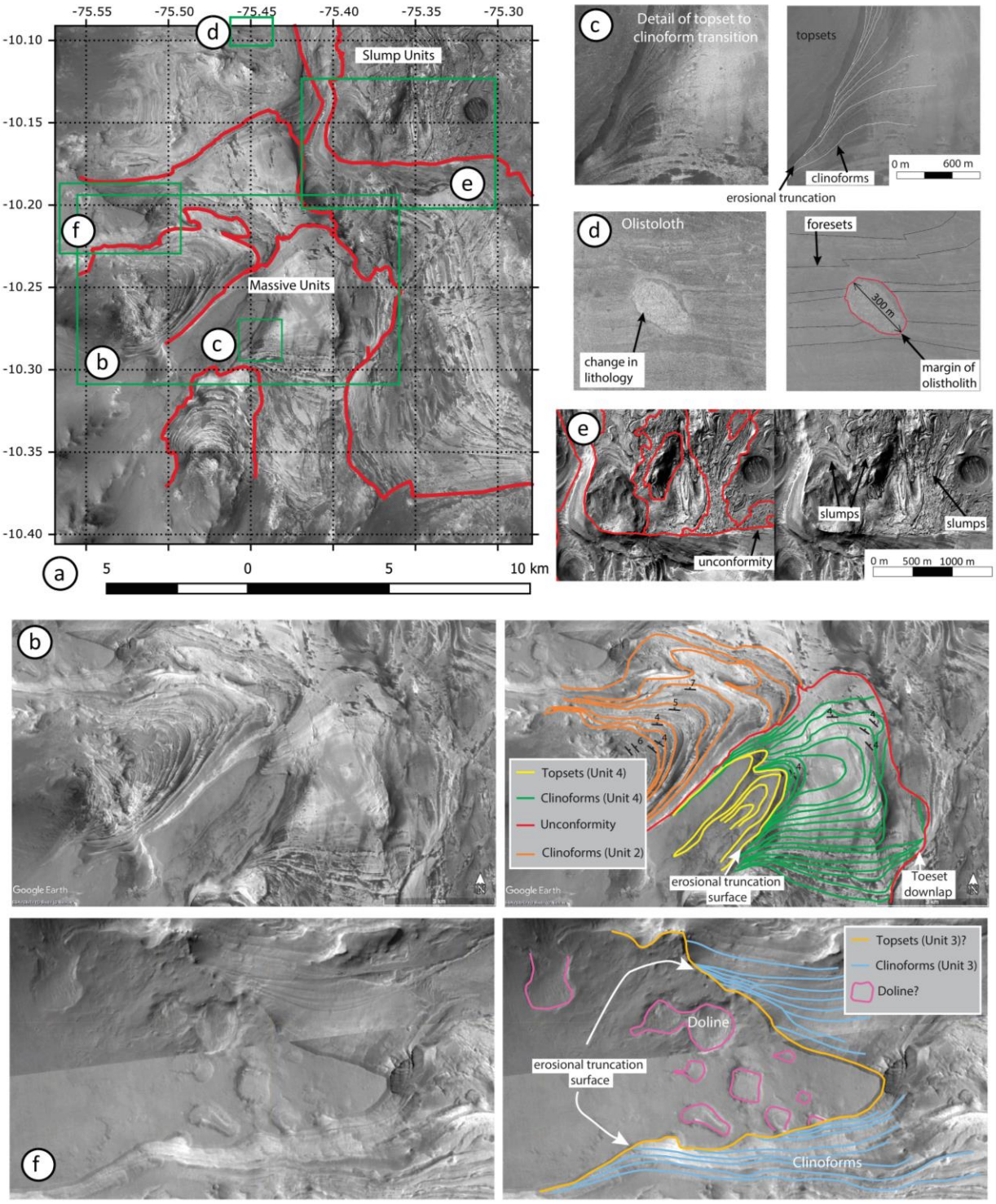

Figure 4: (**a**) CTX image with unconformities marked in red and the classification into young cover, layered units and chaotic units. (**b**) shows a uninterpreted close up of one delta unit and a interpreted close up showing topsets and foresets. (**c**) shows an example for clinoforms (**d**) shows an example for olistoliths (**e**) presents a closeup to the slumped area, and (f) shows a closeup of clinoform to topset relationships and dolines.

285 4.2 Stratigraphic relationships between the high elevation massive layers (Gilbert deltas)

286 Mapping reveals that it is possible to identify four stratigraphic Gilbert delta units
287 (hereafter DU) with seven deltaic lobes (Fig. 3).

288 The lowest stratigraphic unit (DU1) consists of thick beds that are gently folded, and
289 strike on average north-south. The dip is between 3° and 14° towards the east, measured using
290 the three-point approach (Bennison 1990). DU1 underlies the slumped units that are described
291 later, shown by the dip directions and the dip of the unconformity between the two units (Fig. 3).
292 The unconformity also truncates the beds of DU1. DU1 also contains local unconformities that
293 can be traced for a few hundred metres and these are interpreted as local incision related to
294 clinoform migration/avulsion on the delta front and margins. DU1 is at low elevation relative to
295 the other delta units with its uppermost outcrops at -1750 m below the average elevation on Mars
296 (Fig. 3).

297 The next younger unit (DU2), is stacked on top of DU1, and consists of three delta lobes
298 covering areas of between 3-4 km. Two of them in the north of the mapping area appear to be
299 contemporaneous, evidenced by the lateral continuity of layering. We have been unable to map
300 the third lobe laterally to connect with the two other lobes, but we interpreted it to be part of
301 DU2 due to stratigraphic observations described below. DU2 contains large (300 m across) oval
302 shaped blocks, interpreted as olistoliths, that interrupt the bedding structures of the foreset (Fig.
303 4d).

304 The third delta unit (DU3) downlaps onto both DU1 and DU2 and hence stratigraphically
305 overlies them. DU3 is less well exposed that other deltas, only appearing in erosional windows
306 through younger units. There is some evidence for erosional truncation of clinoforms beneath
307 topsets (Fig. 4f). On top of the uppermost layers of DU3, obscured to an extent by younger dust,
308 there are small depressions that do not resemble impact craters because they do not display
309 circular shapes or fringing ejecta deposits, but are similar in shape to terrestrial doline structures.
310 These may have formed during exposure of the delta top (Fig. 4f).

311 Delta unit 4 (DU4) downlaps onto DU1, DU2 and DU3. DU4 shows the clearest example
312 of the relationship between topsets and underlying clinoforms separated by an erosional
313 truncation surface. It also displays the best examples of radial dips revealing the progradation
314 and lateral avulsion directions of the delta. Up-dip clinoform terminations can be best seen in the

top layers of DU4 due to erosional truncation. DU4 is at high elevation relative to the other delta units, with its topsets at -1000 m, some 750 m above the highest outcrops of DU1.

In summary, the 4 delta units are located in what would be the immediate hangingwall of the normal fault that is thought to define the margin of Melas Chasma. The fact that the deltas are stacked on top of each other suggests that if base level, defined by water elevation (e.g. sea-level or lake level) remained relatively constant during sedimentation, there must have been basin subsidence during deposition. This subsidence is consistent with the location in the hangingwall of a normal fault and may suggest that the fault was active during sedimentation. An alternative interpretation could be that water level increased, placing successively younger delta units higher in elevation than older deltas. However, the geometries we have mapped are inconsistent with this interpretation because (a) progressive rise of water level tends to produce retrogradational delta geometries where the points of downlap would progressively move up dip relatively to clinoform surfaces, and not display downdip, basinward migration as observed in individual delta units (Fig. 4b), and (b) this would not produce the observed unconformities. Thus, we are left with the interpretation where base level defined by water elevation remained relatively constant with ongoing fault-related subsidence during deposition. If the base level defined by water elevation remained relatively constant, the ~750 m difference in elevation between the topsets of DU4 and the highest outcrops of DU1 suggest ~750 m fault-related subsidence, which in turn implies a relatively-long history of sedimentation given the slip-rates rates of ~0.1-1 mm per year that typify known normal faults (e.g. Vetterlein and Roberts 2010).

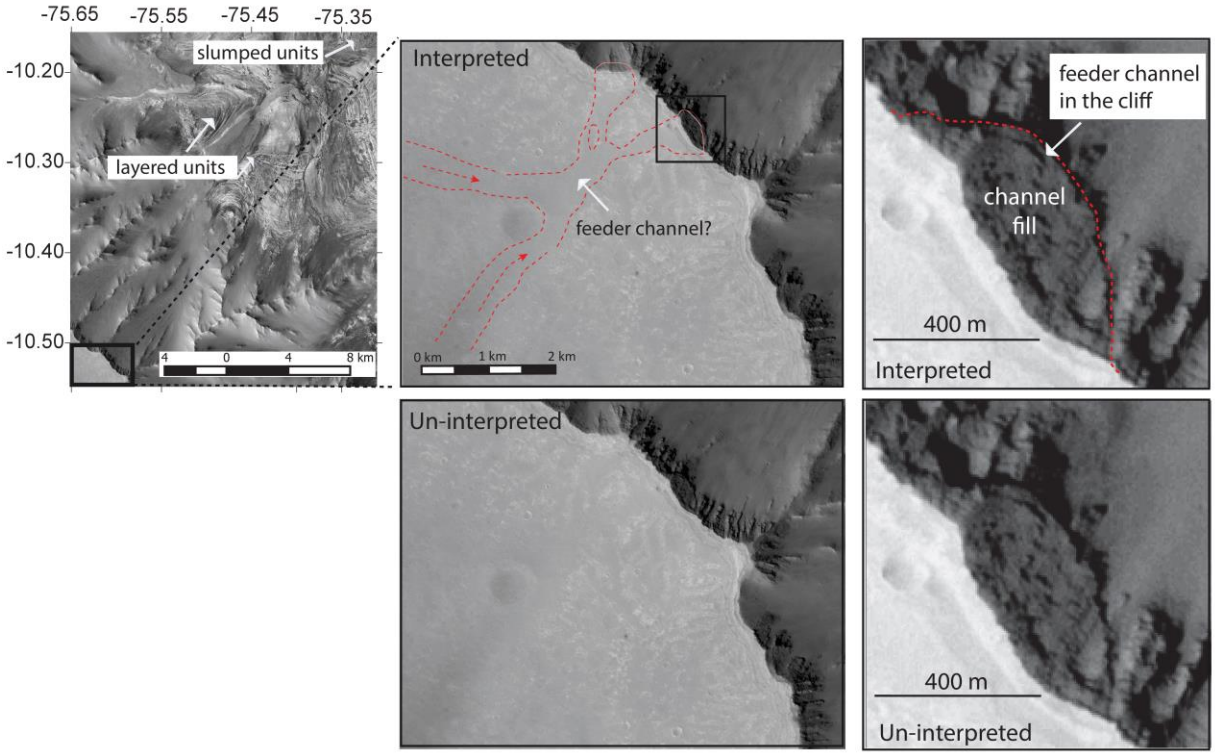

Figure 5: The left figure shows a CTX image of the margin south east of the area of interest. In the figure in the centre is the same imaged zoomed in. Here, the channels can be identified on the plateau.. The lines follow a possible feeder channel that is filled up with material. Zoomed in even further (left image). The different lithology in the slope can be seen. Uninterpreted imagery is provided below the zoomed in images.

4.3 Slumped Area

To the NE and at lower elevations than the Gilbert deltas, an area of the low-relief valley-floor is characterised by relatively thin-bedded layers a few tens to hundreds of metres bed thick, with layers that show variable resistance to erosion (Figs. 3, 4 and 6). The layers have been recognised to be rich in sulphates, evidenced by data from the OMEGA instrument on Mars Express spacecraft (Bibring et al., 2006). The layers are also intensely folded and resemble slump folds (Metz et al. 2010). These authors recognised the origin of these deposits as sedimentary slumps, but did not link their formation to that of deltas at higher elevations as we attempt later in this paper. In some locations it appears that folding is so intense and layers are so thin, that layers and folds appear dismembered, with hook-shaped outcrop patterns where folds appear to have missing limbs (termed “pull-apart” structures by Metz et al. 2010), with these examples surrounded by a matrix within which it has not been possible to identify layering (Fig.

6d). The intense folding, combined with the low relief, means that we have not been able to measure values for dip. However, it is clear that the fold patterns indicate the existence of juxtaposed antiforms and synforms. In some locations it is also clear that the fold axial surfaces are non-planar, and curve around later fold axial traces, indicating the existence of polyphase fold structures (Fig. 6e). Polyphase structures are common within areas of sedimentary slumping (Alsop, Marco, Weinberger, & Levi, 2016). These structures are well displayed in HiRISE image ESP_019442_1700.

We have mapped the folds across the region and determined the stratigraphic relationships between the slumped units and the delta units. Where fold axial traces lie across strike from one another, and layers can be traced continuously between the adjacent folds, we use the principle that there must be a strict sequence from antiform-to-synform-to-antiform-to-synform. This sequence, combined with observations of shadows on the images that in places help to decide dip direction, and the sequence of re-folding of axial traces, have allowed us to determine which folds are antiforms and synforms and the stratigraphic relationships between the delta units, and within the slumped units.

The slumped units unconformably overlie the clinoforms of DU1 evidenced by a sharp, unconformable contact visible on the images (Fig. 6f). The stratigraphic relationship between the slumped units and the other delta units is more challenging to establish. We have been unable to find a contact between them on the imagery. However, the proximity between slumped units and the other delta units is only <~1km in the north of the area (Fig. 3), and they are similar elevations, so cross-section construction suggested that the unconformity beneath the slumped unit may be the continuation of the composite unconformity formed from the juxtaposition of the unconformities separating DU1, DU2, DU3 and DU4. Thus, our interpretation is that the slumped units are the lateral equivalents of DU2, DU3 and DU4 (Fig. 3).

Furthermore, inside the slumped area three stratigraphic units were identified separated by unconformities, and their relative ages were established. The different slumped units show different properties. Slumped unit 2 (SU2) has characteristic disrupted beds with hook-shaped dismembered folds, where individual layers are so deformed and chaotic that single horizons cannot be traced. The next younger unit, slumped unit 3 (SU3), shows thin beds that are tightly folded. The beds alternate between slightly thicker light layers and thinner dark layers. F1 and

F2-folds are well preserved in this unit. In slumped unit 4 (SU4) the layers are thicker, and contain less of the darker thinner layers, and appear more resistant to erosion. The layers may be more competent as they are less tightly folded compared to SU3 and F1-folds dominate the structure. The different properties of the three different slumped units helped to confirm the existence of synforms and antiforms, for example the repetition of SU4 at the surface along the profile line A-B (Fig. 6). The slumped unit that is lateral equivalent of DU1, if it exists, may be in the sub-surface. We note that F1 folds are present in the youngest slump unit (SU4), so F1 folds and all later fold phases, formed after deposition of the entire sequence of slumped units, implying they were able to maintain their propensity to slump folding throughout deposition; this could be due to a combination retention of an unlithified state, perhaps due to water retention, or perhaps due to the low yield strength of sulphate-rich sediments.

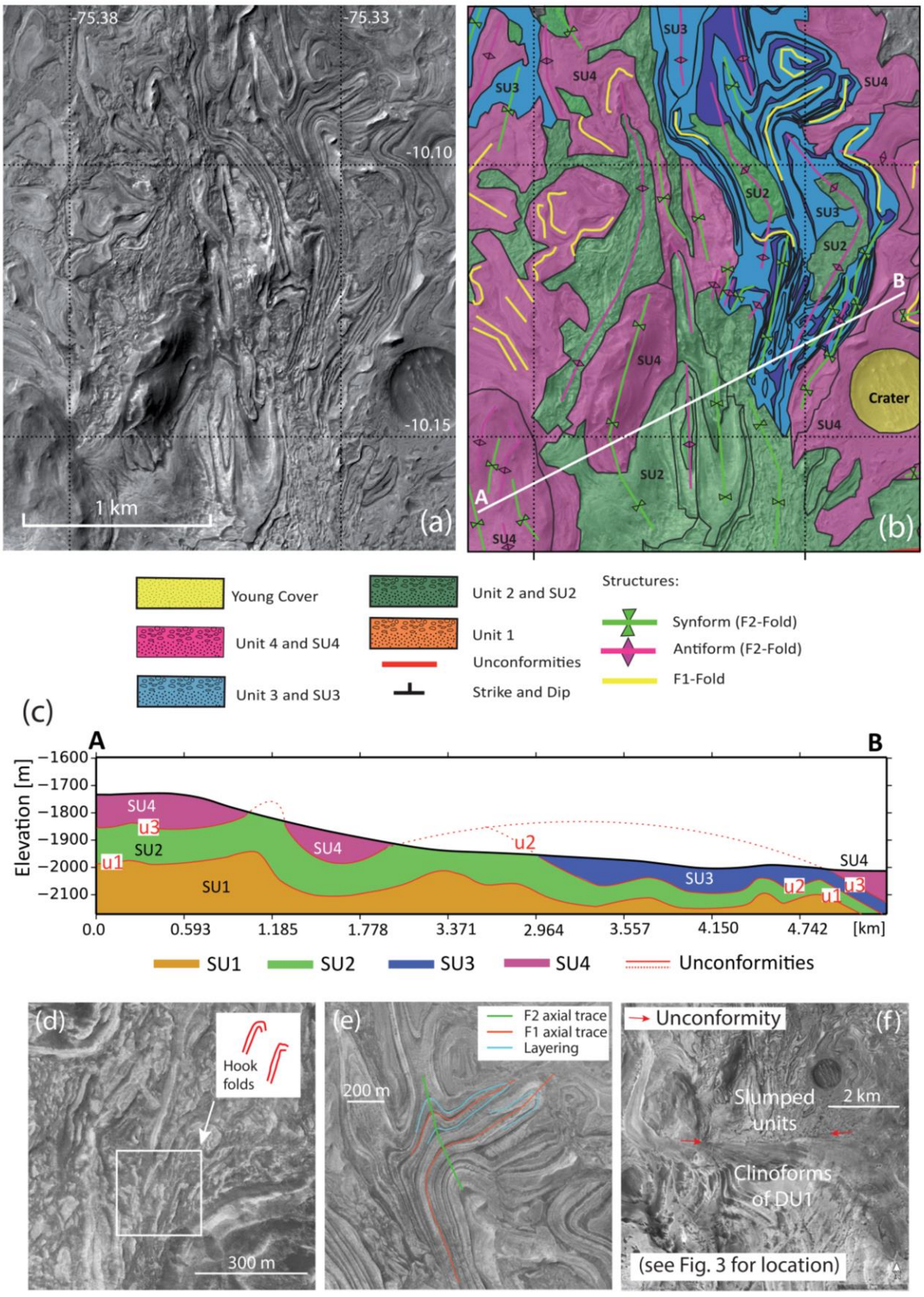
-75.38
-75.33
-10.10
-10.15
1 km
(a)
SU3
SU4
SU2
Crater
A
B
(b)
Young Cover
Unit 4 and SU4
Unit 3 and SU3
Unit 2 and SU2
Unit 1
Unconformities
Strike and Dip
Structures:
Synform (F2-Fold)
Antiform (F2-Fold)
F1-Fold
(c)
Elevation [m]
−1600
−1700
−1800
−1900
−2000
−2100
u1
u2
u3
SU1
SU2
SU3
SU4
0.0
0.593
1.185
1.778
3.371
2.964
3.557
4.150
4.742
[km]
Unconformities
(d)
Hook folds
300 m
(e)
F2 axial trace
F1 axial trace
Layering
200 m
(f)
Unconformity
Slumped units
2 km
Clinoforms of DU1
(see Fig. 3 for location)

393

Figure 6 (**a**) shows uninterpreted imagery of the region of interest. (**b)** A detailed map of the slumped area in the mapping region is shown in this figure. With the help of the deformation features a possible stratigraphic relation was established and illustrated in the profile **(c).** More detailed features are shown e.g. in (**d**) hook folds., (**e**) polyphase fold structures, and (**f**) clear unconformable contact.

Overall, the dip of the units to the northeast in the mapping area suggests an overall decrease in age of the layers towards the east, confirmed by our mapping. The most western unit (SU4) in the slumped area forms a syncline followed by an anticline in the neighbouring unit (SU2) to the west. Because the western slumped unit (SU4) is located in the centre of the synform whereas the bordering unit (SU2) is located in the centre of an anticline, it is implied that the western slumped unit (SU4) is expected to be younger than the bordering one (SU2). At the next unconformity in the east an antiform is in the west, in the disrupted unit (SU2), and a synform in the east of the unconformity, in the closely folded unit (SU3). This indicates that the disrupted unit (SU2) in the west is older than the neighbouring closely folded unit (SU3). The same situation can be observed further east where SU3 borders to a younger unit in the east. As a result, the most eastern unit is younger than the closely folded unit (SU3).

The most eastern and western units are interpreted as the same unit (SU4), because of their similar texture, magnitude of deformation, and the stratigraphic relationships we have mapped. Furthermore, note the existence of features in SU2, 3 and 4 that are erosional windows and inliers. An erosional inlier formed on SU2. In the middle of SU2 there is an oval outcrop of SU4 located along a syncline axis. Because of the formation of syn- and antiforms, the younger unit (SU4) only remained in the synforms and was eroded at the big antiforms. Similar observations can be made in SU3 where two oval areas of SU2 outcrop along an anticline axis. The windows were related to each of their units by comparing their texture and deformation features.

4.4 Summary

Overall, the observations in this work suggest 4 stacked delta units consisting of topsets, foresets with clinoforms with downlapping geometries, and olistoliths. The slumped units are the lateral equivalents of these delta units. This implies the sediments were deposited into a body of water with a water level equivalent to the elevation difference between the shallow-water topsets and the deeper-water basinal slumped units; for Unit 4 this is an elevation difference of 600-700

metres (Fig. 3). Figure 7 provides a schematic summary of these observations. To further elucidate the significance of the sedimentary features in Melas Chasma, below we describe terrestrial analogues from the Gulf of Corinth, Greece, which is characterised by stacked deltas in the hangingwalls of active normal faults.

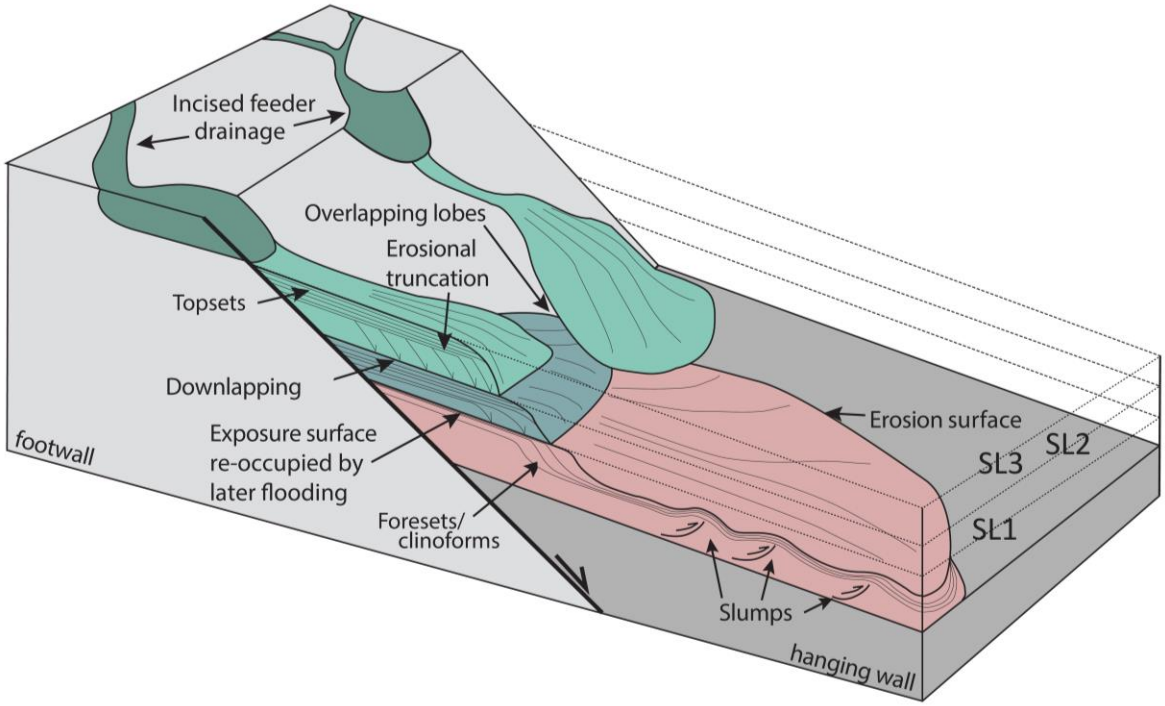

Figure 7: Schematic block sketch of stacked deltas on a hangingwall of a normal fault.

5 Comparison with the Gulf of Corinth

The Gulf of Corinth appears to be a terrestrial analogue example for the stacked deltas in Melas Chasma because on its southern coastal region, deltas were exhumed during Quaternary fault-related uplift, exposing several sequences of stacked Gilbert-type deltas located in the hangingwalls of faults older faults. These examples for the Gulf of Corinth have been described in a number of papers after detailed mapping (Backert et al., 2010; Dart et al., 1994; Ford et al., 2007; Gawthorpe et al., 2017; Ori, 1989; Rohais et al., 2008). We conducted fieldwork to examine the stacked deltas, and in the following, observations from the Kerinitis delta will be reviewed and described, and used to help interpret the examples from Melas Chasma.

The Gulf of Corinth is an active rift system located in western Greece that has been active for ~5 Ma (Backert et al., 2010; McNeill & Collier, 2004). Northwards dipping, right stepping

normal faults produce half-graben structures, which have been extending since the Pliocene and are still spreading today, due to back arc spreading (McNeill & Collier, 2004; Ori, 1989; Roberts & Jackson, 1991; Rohais et al., 2008). The west-northwest to east-southeast trending rift system continues for ca. 100 km and is 25-30 km wide forming an asymmetric graben (Dart et al., 1994; Roberts & Jackson, 1991; Rohais et al., 2008).

The geologic history of the Gulf of Corinth can be divided into two phases, according to Ori (1989). During the first phase of low subsidence rates, the basin was filled with continental, and shallow water sediments. With the second phase, this changed dramatically. During high rates of subsidence, deep-sea sediments and Gilbert-type deltas were deposited with a thickness of several hundreds of meters (Ford et al., 2007; Ori, 1989).

The Kerinitis delta is a coarse-grained stacked Gilbert-type delta, located in the hangingwall of the Pyrgaki-Mamoussia fault, which was active in the lower Pleistocene, and the footwall of the still active Agion fault (Backert et al., 2010). It was deposited between the Early and early Middle Pleistocene and later uplifted as fault activity migrated to the north. Thus, the uplift of former hangingwall blocks is caused by a northwards migration of the active faulting and river incision has exposed the stacked deltas (Dart et al., 1994; Ori, 1989). The Kerinitis delta has a radius of 3.8 km and a thickness over 600 m, but this is comprised of stacked deltas; individual deltas are on the order of tens of metres to a few hundred metres thick (Backert et al., 2010; Dart et al., 1994; Gawthorpe et al., 2017). Deposition during the middle and late Pleistocene was affected by glacio-eustatic sea-level fluctuations produced by changes in ice volume at the Earth's poles (Dart et al. 1994). In the Late Pleistocene sea-levels fluctuated by ~100-120m on ~100-125 kyrs cycle, although there are shorter timescale cycles superimposed on this pattern. These sea-level fluctuations combined with the vertical slip-rates on the faults of ~0.5-1.0 mm/yr means that individual deltas formed at interglacial sea-level highstands, were sub-aerially exposed during lowstands during glacial periods, and subjected to hangingwall subsidence of ~50-100 metres before the subsequent interglacial highstand; sea-level from the subsequent highstand therefore flooded over the top-sets of previous deltas and submerged them by tens of metres. The tens of metres of accommodation space was filled by delta progradation with clinoforms downlapping onto the topsets of former deltas. Incised drainage formed during lowstands were infilled by marine sediments during sea-level rise and subsequent highstand. Thus, the combination of sea-level fluctuations and ongoing fault-related hangingwall

subsidence produced a series of stacked deltas. Deposits on the basin floor are less-well exposed as they are mainly submerged beneath the present-day Gulf of Corinth, but the limited outcrops that do exist are fine grained carbonate marls which in places display centimetre to metre-scale slump folding.

The geometry of the Kerinitis delta shows the expected structure of a delta on a hangingwall (Fig. 8). There have been 12 stacked delta sequences identified in the literature. The sediment are bedded, some layers are sub-horizontal, dipping slightly to the south in the southeast of the outcrop. The other type of layers dips steeply, ~20°, to the northeast. These layers consist of sandy coarse conglomerates, including boulders. The clasts consist mainly of limestone, radiolarite, and sandstones. The existence of karst caves indicates a carbonate binding material.

Foresets show typical clinoform structures. The topsets are mainly alluvial, but are shallow marine at some locations. A detailed description of the different delta facies was done by Backert et al. (2010). The sequence boundaries can be identified by unconformities due to e.g. downlap structures, and a shift of the topset breaking point. The sequences are composite type 1 and type 2 boundaries. Eleven sequence boundaries have been identified (Fig. 8), representing abrupt eustatic sea-level rises, separating twelve stratigraphic units; these are interpreted as eustatic water level regression.

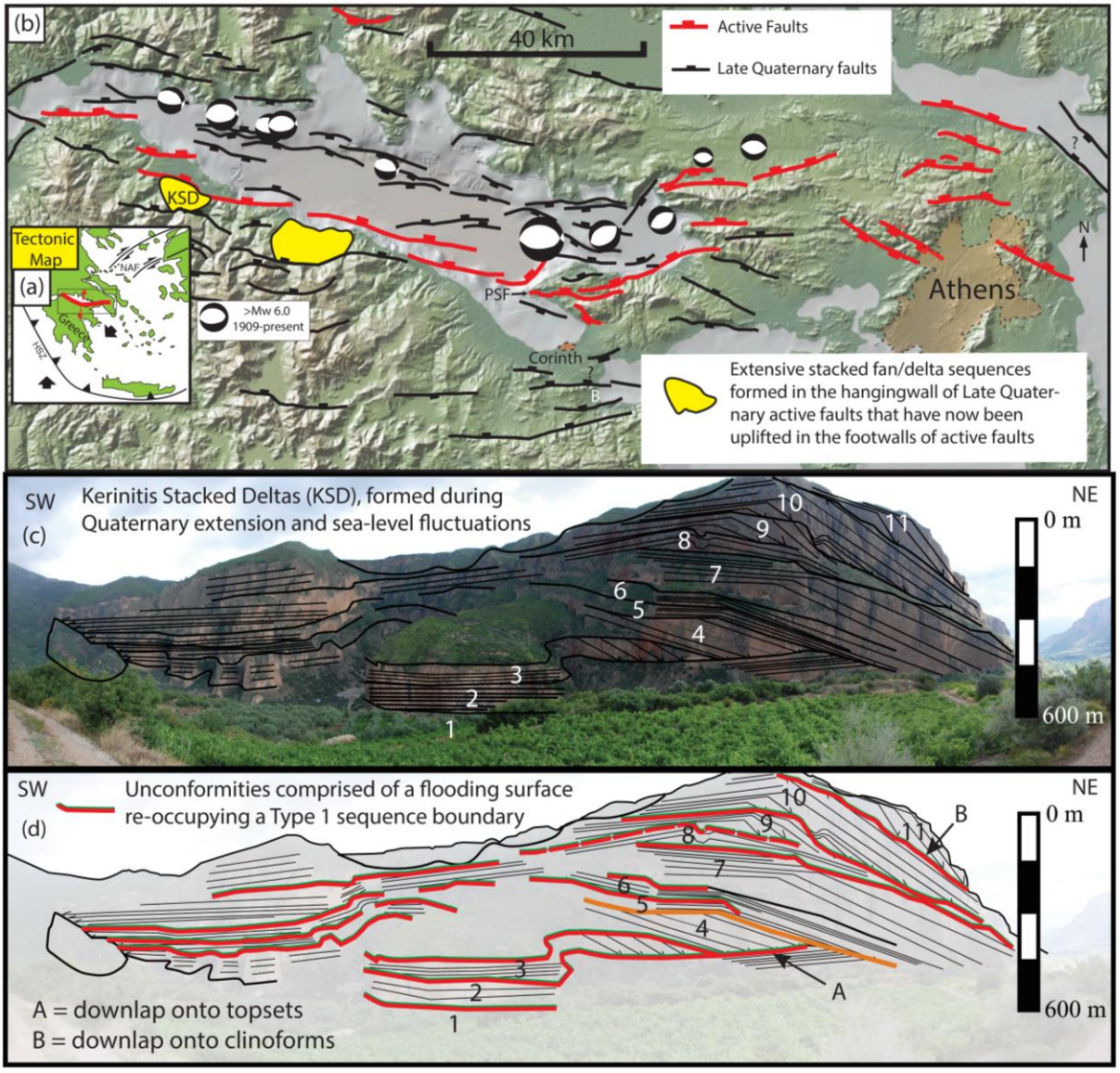

Figure 8: (**a**) shows a small scale tectonic map of Greece. (**b**) shows a tectonic map of the Gulf of Corinth. (**c**) shows a panorama collage of the 600 m high outcrop of the Kerinitis delta. (**d**) The sequence boundaries can be seen clearly at this location and stacked, and erosional patterns can be recognized. The different sequences and their patterns are sketched here. The different sequences are prograding towards the basin in the northeast and are interrupted by type 2 sequence boundaries causing stacked patterns. There is a type 1 boundary, an erosion surface, marked by the orange line, where sequences were partly eroded.

In summary, the key features that resemble the deposits in Melas Chasma, and aid in their interpretation are as follows; (1) The existence of a tripartite subdivision into topsets, clinoforms

and toesets; (2) The existence of downlap surfaces where downdip clinoform terminations directly overlie topsets or clinoform deposits; (3) The existence of stacked delta deposits.

6 Discussion

6.1 Delta Deposit Geometry

The observations and interpretations in this work show several delta lobes stacked above each other, located on a normal fault. The different layers show the typical delta geometries, clinoforms in foresets, topset and a downdip relation to lower shelf facies in form of slumps. Terrestrial examples like the Kerinitis delta show similar key features such as topsets, clinoforms with sequences downlapping on older topsets and foresets. The slumped area in Melas Chasma cannot directly be correlated with the delta lobes as all contacts between the two deposits show unconformities. But the slumps location, downdip of the deltas indicates a stratigraphic connection and there are examples on Earth, where slope collapses of hardly solidified sediments cause folding in the deposits leaving slumped areas (Alsop et al., 2016). The symmetry of the deposits in Melas Chasma and their comparison to terrestrial examples lead to the conclusion that these deposits are delta deposits that are linked to slumps further downslope. The link between these deltas and slumps as their toesets suggests a water body several hundred metres deep.

Further indicators that the sediments were deposited on the margin of a shelf are the observed olistoliths. They are the result of a gravity mass transport that transported the olistolith downslope and deposited it in normal layered sediments (Cieszkowski et al., 2009; Ślączka, Renda, Cieszkowski, Golonka, & Nigro, 2012). They are common in terrestrial shelf facies and transported by submarine debris flows, triggered by tectonic activity. They can reach sizes of several kilometres in diameter and interrupt the bedding of shelf sediments. Examples for olistoliths can be found in deep water sediments (Heubeck, 1992), but also for example in alluvial fans filling graben structures (Seidel, Seidel, & Stöckhert, 2007). The examples we have identified in Melas Chasma are ~300 m across, and must have been transported for hundreds of metres evidenced by the mismatch in lithologies between the olistoliths and surrounding matrix. Thus, it is hard to imagine how such blocks could have been transported without the aid of water.

Therefore, the presence of olistoliths suggests to us that subaqueous conditions prevailed during the transport and deposition of the olistoliths and surrounding matrix.

Overall, our interpretation suggests that to allow delta deposits to develop a large water body over an extended period of time is necessary. This implies the existence of a several hundreds of metres deep paleolake or ocean reaching into Melas Chasma.

6.2 Delta Evolution and Controls

In the area of study, the unconformities between the different lobes and the stratigraphic relations imply a period of erosion or non-deposition after the deposition of the sequences, followed by rapid relative sea-level rises leading to the stacked geometries of the different lobes above each other.

The geometry of deltas located at a hangingwall of a normal fault is influenced by various factors, such as the fault slip-rate, accommodation space and sediment supply. Sediment supply depends on the drainage system upstream and climatic influences. Accommodation space is created by subsidence, which is expected to be the dominant process in the hangingwall of a normal fault, assuming constant slip-rates along the fault. Eustatic water level fluctuation can increase the creation of accommodation over a relative short period of transgression, but can also reduce slowly the accommodation space during a usually longer lasting period of regression (Backert et al., 2010; Gawthorpe et al., 2003); it is this water-level variation that is perhaps the most intriguing and difficult to resolve for the examples in Melas Chasma. Our interpretation is as follows:

1) The tripartite division into topsets, clinoforms and toesets suggests that each of the 4 delta sequences were deposited in a body of water several hundred metres deep, with the slumped units representing the basin-floor, deeper-water sedimentation.
2) Delta units have been progressively downthrow by ongoing fault activity evidenced by clinoforms downlapping onto older delta sequences.
3) In turn point (2) implies that water-level rose above the top-sets of previous deltas.
4) The reason why water-level rose above previous top-sets could be solely due to fault-related subsidence, but there a few intriguing observations that may also point to eustatic water-level fluctuations. Firstly, we observe that DU3 may be inset, in terms of elevation,

down between two delta lobes from DU2, but it lacks clear topsets so it is challenging to conclude on this point; this may be signs of a lowered base-level, but the evidence is not completely compelling; we also lack observations of incised and infilled drainage channels that would needed to support this point (see Fig. 2). Secondly, we have observed structures that resemble dolines. Terrestrial examples of dolines in sulphate rich deposits occur where sub-aerial exposure allows dissolution of sulphate in the shallow-sub-surface (Klimchouk, Forti, & Cooper, 1996), and similar features have been reported from Mars (Baioni & Tramontana, 2015; Baioni & Tramontanaa, 2017). It may be that the dolines we report were sub-aerially exposed. For this to occur with a background of ongoing subsidence in the hangingwall of a normal fault requires a eustatic water-level fall. Thus, the dolines may provide some evidence that eustatic water-level falls may have occurred, hinting at possible climatic changes on Mars during the ongoing faulting and sedimentation; this is similar to the interpretation for the Gulf of Corinth, but needs further study.

The slumped area in Melas Chasma shows various stages of deformation, represented by F1- and F2-faults that have been mapped. Multiple stages of slumping are also observed in the Dead Sea deposits, where sulphate-rich, and aragonitic basinal deposits have been downthrown by faulting (Alsop et al., 2016). They show fold axis in different orientations, explained by different stages of slumping and reactivation of the faults in the slumped area. We suggest that similar processes have occurred in Melas Chasma. The stacking geometry and the similarity of the deposits to the deltas at the Gulf of Corinth implies a similar tectonic environment in Melas Chasma and at the Gulf of Corinth. Further, the multiple stages of slumping observed in Melas Chasma would support the idea of an active normal fault as a trigger for slumping events. These conclusions are consistent with the hypothesis of deposition on the hangingwall of an active normal fault.

6.3 Timescale

Determining the duration of an alluvial/lacustrine system on Mars is difficult because of lack of data. The duration of the Jezero Crater lake was estimated to be 1-10 Ma, by using terrestrial rates of sediment supply to interpolate the necessary time to deposit the sediment thickness that can be observed (Schon, Head, & Fassett, 2012). Other studies indicate that most

paleo-lakes formed by short periods of flow or groundwater discharge rather than a long sustained river system (Cabrol & Grin, 1999).

It is difficult to reconstruct the timescale from the Melas Chasma deposits alone as they have not been dated directly, but an indication of timescale can be gained from the observation of stacked and offset delta sediments. The total thickness of these stacked deltas in Melas Chasma is at least 1500 m. Looking at smaller terrestrial examples like the Kerinitis delta in similar settings, the deposition of stacked deltas of several hundreds of meters needed several hundred thousands of years (Backert et al., 2010; Rohais et al., 2008). For the area of study, the rates of the normal fault are unknown, therefore slip-rates of terrestrial faults are used as an indicator. The Gulf of Corinth is a fast spreading rift system and the faults have slip-rates between 0.75 and 1.2 mm/a (Backert et al., 2010; McNeill & Collier, 2004). Using a conservative approach and therefore using the faster slip rates, means that at a slip rate of 1.2 mm/a the deposition of 1500 m of sediment would have taken 1.25 Ma.

A study on Martian slip-rates at the northern Cerberus Fossae graben system, using crater count ages, indicates slip-rates between 0.0014 and 0.73 mm/a (Vetterlein & Roberts, 2010). Assuming slip-rates between 0.1 and 0.7 mm/a for the fault system in the area of study gives the deltas a time of deposition of 2.06 to 15 Ma. The results of this study imply that a large body of water must have at least existed for 1.25 Ma, using very fast slip-rates from the Gulf of Corinth on Earth, and between 2.06 Ma to >15 Ma using Martian slip-rates in Cerberus Fossae, which is much longer than suggested by other studies for water bodies on the Martian surface.

6.4 Regional implications

The feeder channel at the rift margin in the southwest of the mapping area connects the area of this study with layered deposits covering the outside plateau of Valles Marineris described by L. Le Deit et al. (2010). They describe the layered deposits as air-fall dust or volcanic ash deposits with water/ice filled pores. The layered deposits were deposited during the Early and Late Hesperian. They show layers rich in opaline silica, aluminium phyllosilicates or hydroxylated ferric sulphates and were periodically eroded by fluvial activity (L. Le Deit et al., 2010). These layered deposits might be a source of the sediments supply forming the deltas inside Melas Chasma assuming they were formed contemptuous to the rift formation in the Early Hesperian.

The paleo water level inferred by the height of the observed topsets allows a connection to a possible ocean on the northern hemisphere (Fig. 1) that has been already postulated in the literature (Barker & Bhattacharya, 2017; Parker et al., 1989). The regional topography is much lower than the height of the topsets. This suggests a water depth of ca. 3000 m for such an ocean. The existence of a deep, long-lived water body has an impact on the view of Martian paleo-climate. The results of this study indicate a significant longer time span for liquid water on the Martian surface. A deep, long lived water body might have insured stable conditions long enough for the development of life. On Earth life in form of bacteria is thought to have developed along the mid-ocean ridges (Martin, Baross, Kelley, & Russell, 2008). Similar conditions might have been provided on Mars inside a large body of water in Valles Mariners.

7 Conclusions

The mapped area in this thesis includes sedimentary deposits with typical Gilbert-type delta geometries, including topsets and foresets. Contemporaneous slumped sediments are located downdip of these deltas and stratigraphically linked as toesets. The deltas are stacked above each other with a total thickness of at least 1500 m, and clinoform dimensions suggest the presence of a large water body, several hundreds of metres deep, on the Martian surface.

The deposit geometries suggest that the sediments were deposited on the hangingwall of an active normal fault. Using sequence stratigraphy, slip rates, and comparisons to terrestrial examples, it was possible to establish a timescale in this research. The results suggest a large body of water on Mars that was stable between 1.25 and 15 million years and was formed while the rift was active. Similar formations on Earth that can be used as analogue examples agree with this interpretation.

A large water body in Valles Marineris could most likely be connected to an ocean on the northern hemisphere of Mars, as Valles Marineris is topographically connected to the northern plains by channels leading to the northern basin, passing streamlined islands. The indicated water level in Melas Chasma would suggest water depths of ca 3 km of such an ocean.

Open Research Data

Datasets for elevation information in this research are available in these in-text data citation references: Fergason et al., 2018. Further data were not used, nor created for this research.

References

Alsop, G. I., Marco, S., Weinberger, R., & Levi, T. (2016). Sedimentary and structural controls on seismogenic slumping within mass transport deposits from the Dead Sea Basin. *Sedimentary Geology*, *344*, 71–90. https://doi.org/10.1016/j.sedgeo.2016.02.019

Anderson, R. B., & Bell III, J. F. (2010). Geologic mapping and characterization of Gale Crater and implications for its potential as a Mars Science Laboratory landing site. *Mars*, *5*, 76–128.

Backert, N., Ford, M., & Malartre, F. (2010). Architecture and sedimentology of the Kerinitis Gilbert-type fan delta, Corinth Rift, Greece. *Sedimentology*, *57*(2), 543–586.

Baioni, D., & Tramontana, M. (2015). Evaporite karst in three interior layered deposits in Iani Chaos, Mars. *Geomorphology*, *245*, 15–22. https://doi.org/10.1016/j.geomorph.2015.05.018

Baioni, D., & Tramontanaa, M. (2017). Possible evaporite karst in an interior layered deposit in Juventae Chasma, Mars. *International Journal of Speleology*, *46*(2), 181.

Barker, D. C., & Bhattacharya, J. P. (2017). Sequence stratigraphy on an early wet Mars. *Planetary and Space Science*.

Bartov, Y., Stein, M., Enzel, Y., Agnon, A., & Reches, Z.'e. (2002). Lake Levels and Sequence Stratigraphy of Lake Lisan, the Late Pleistocene Precursor of the Dead Sea. *Quaternary Research*, *57*(01), 9–21. https://doi.org/10.1006/qres.2001.2284

Bennison, G. M. (1990). 'Three-point'problems. In G. M. Bennison (Ed.), *An Introduction to Geological Structures and Maps* (pp. 11–15). Springer.

Bibring, J.-P. [Jean-Pierre], Langevin, Y., Mustard, J. F. [John F.], Poulet, F. [François], Arvidson, R. [Raymond], Gendrin, A. [Aline], . . . Forget, F. (2006). Global mineralogical and aqueous Mars history derived from OMEGA/Mars Express data. *Science*, *312*(5772), 400–404.

Cabrol, N. A., & Grin, E. A. (1999). Distribution, classification, and ages of Martian impact crater lakes. *Icarus*, *142*(1), 160–172.

Carr, M. H. (2003). Oceans on Mars: An assessment of the observational evidence and possible fate. *Journal of Geophysical Research*, *108*(E5). https://doi.org/10.1029/2002JE001963

Cieszkowski, M., Golonka, J., Krobicki, M., Slaczka, A., Oszczypko, N., Waskowska, A., & Wendorff, M. (2009). The Northern Carpathians plate tectonic evolutionary stages and origin of olistoliths and olistostromes. *Geodinamica Acta*, *22*(1-3), 101–126. https://doi.org/10.3166/ga.22.101-126

Craddock, R. A., & Howard, A. D. (2002). The case for rainfall on a warm, wet early Mars. *Journal of Geophysical Research: Solid Earth*, *107*(E11).

Dart, C. J., Collier, R. E. L. [Richard E. Ll], Gawthorpe, R. L. [Rob L.], Keller, J. V. A., & Nichols, G. [Gary] (1994). Sequence stratigraphy of (?) Pliocene-Quaternary synrift, Gilbert-type fan deltas, northern Peloponnesos, Greece. *Marine and Petroleum Geology*, *11*(5), 545–560.

Davis, J. M. [J. M.], Grindrod, P. M. [P. M.], Fawdon, P. [P.], Williams, R. M. E. [R. M. E.], Gupta, S. [S.], & Balme, M. [M.] (2018). Episodic and Declining Fluvial Processes in Southwest Melas Chasma, Valles Marineris, Mars. *Journal of Geophysical Research: Planets*, *123*(10), 2527–2549. https://doi.org/10.1029/2018JE005710

Davis, J. M. [Joel Michael] (2017). *The Geology of Ancient Fluvial and Lacustrine Systems in Arabia Terra and Melas Chasma, Mars.* UCL (University College London).

Dromart, G. [Gilles], Quantin, C. [Cathy], & Broucke, O. (2007). Stratigraphic architectures spotted in southern Melas Chasma, Valles Marineris, Mars. *Geology*, *35*(4), 363. https://doi.org/10.1130/G23350A.1

Fawdon, P. [Peter], Gupta, S. [Sanjeev], Davis, J. M. [Joel M.], Warner, N. H., Adler, J. B., Balme, M. R., . . . Sefton-Nash, E. (2018). The Hypanis Valles delta: The last highstand of a sea on early Mars? *Earth and Planetary Science Letters*, *500*, 225–241. https://doi.org/10.1016/j.epsl.2018.07.040

Feldman, W. C., Prettyman, T. H., Maurice, S., Plaut, J. J., Bish, D. L., Vaniman, D. T., . . . Karunatillake, S. (2004). Global distribution of near-surface hydrogen on Mars. *Journal of Geophysical Research: Solid Earth*, *109*(E9).

Fergason, R.L., Hare, T. M., & Laura, J. (2018). HRSC and MOLA Blended Digital Elevation Model at 200m v2. Retrieved from http://bit.ly/HRSC_MOLA_Blend_v0

Ford, M., Williams, E. A., Malartre, F., Popescu, S.-M., Nichols, G. [G.], Williams, E. [E.], & Paola, C. (2007). Stratigraphic architecture, sedimentology and structure of the Vouraikos Gilbert-type fan delta, Gulf of Corinth, Greece. *Sedimentary Processes, Environments and Basins: A Tribute to Peter Friend: Oxford, Blackwell Publishing Ltd*, 49–90.

Forsberg-Taylor, N. K., Howard, A. D., & Craddock, R. A. (2004). Crater degradation in the Martian highlands: Morphometric analysis of the Sinus Sabaeus region and simulation modeling suggest fluvial processes. *Journal of Geophysical Research: Solid Earth*, *109*(E5).

Gawthorpe, R. L. [R. L.], Andrews, J. E., Collier, R. E. L. [Richard E. L.], Ford, M., Henstra, G. A., Kranis, H., . . . Skourtsos, E. (2017). Building up or out? Disparate sequence architectures along an active rift margin—Corinth rift, Greece. *Geology*, *45*(12), 1111–1114.

Gawthorpe, R. L. [R. L.], Colella, A., & Prior, D. B. (1990). Tectonic controls on coarse-grained delta depositional systems in rift basins. *Coarse-Grained Deltas*, 113–127. Retrieved from https://books.google.de/books?hl=de&lr=&id=L8_zP9vXxrAC&oi=fnd&pg=PA113&dq=gawthorpe+colella+tectonic+controls&ots=Hkc0SsqRBe&sig=lI5tPZ2u7n_eCOkSQBJ35xFCYIo#v=onepage&q=gawthorpe%20colella%20tectonic%20controls&f=false

Gawthorpe, R. L. [R. L.], Fraser, A. J., & Collier, R. E.L. (1994). Sequence stratigraphy in active extensional basins: implications for the interpretation of ancient basin-fills. *Marine and Petroleum Geology*, *11*(6), 642–658. https://doi.org/10.1016/0264-8172(94)90021-3

Gawthorpe, R. L. [R. L.], Hardy, S., & Ritchie, B. (2003). Numerical modelling of depositional sequences in half-graben rift basins. *Sedimentology*, *50*(1), 169–185. https://doi.org/10.1046/j.1365-3091.2003.00543.x

Gilbert, G. K. (1885). *The topographic features of lake shores*: US Government Printing Office.

Grotzinger, J. P., Gupta, S. [S.], Malin, M. C. [M. C.], Rubin, D. M. [D. M.], Schieber, J., Siebach, K., . . . Arvidson, R. E. (2015). Deposition, exhumation, and paleoclimate of an ancient lake deposit, Gale crater, Mars. *Science*, *350*(6257), aac7575.

Gwinner, K., Scholten, F., Spiegel, M., Schmidt, R., Giese, B., Oberst, J., . . . Neukum, G. (2009). Derivation and validation of high-resolution digital terrain models from Mars Express HRSC data. *Photogrammetric Engineering & Remote Sensing*, *75*(9), 1127–1142.

Head, J. W., Hiesinger, H., Ivanov, M. A., Kreslavsky, M. A., Pratt, S., & Thomson, B. J. (1999). Possible ancient oceans on Mars: evidence from Mars Orbiter Laser Altimeter data. *Science*, *286*(5447), 2134–2137.

Heubeck, C. (1992). Sedimentology of Large Olistoliths, Southern Cordillera Central, Hispaniola. *SEPM Journal of Sedimentary Research*, *Vol. 62*. https://doi.org/10.1306/D4267929-2B26-11D7-8648000102C1865D

Klimchouk, A., Forti, P., & Cooper, A. (1996). Gypsum karst of the World: a brief overview. *International Journal of Speleology*, *25*(3), 12.

Le Deit, L. [L.], Bourgeois, O., Mège, D. [D.], Hauber, E. [E.], Le Mouélic, S., Massé, M., . . . Bibring, J.-P. [J.-P.] (2010). Morphology, stratigraphy, and mineralogical composition of a layered formation covering the plateaus around Valles Marineris, Mars: Implications for its geological history. *Icarus*, *208*(2), 684–703. https://doi.org/10.1016/j.icarus.2010.03.012

Le Deit, L. [Laetitia], Hauber, E. [Ernst], Fueten, F., Pondrelli, M., Rossi, A. P., & Jaumann, R. [Ralf] (2013). Sequence of infilling events in Gale Crater, Mars: Results from morphology, stratigraphy, and mineralogy. *Journal of Geophysical Research: Planets*, *118*(12), 2439–2473. https://doi.org/10.1002/2012JE004322

Liu, Y., & Catalano, J. G. (2016). Implications for the aqueous history of southwest Melas Chasma, Mars as revealed by interbedded hydrated sulfate and Fe/Mg-smectite deposits. *Icarus*, *271*, 283–291. https://doi.org/10.1016/j.icarus.2016.02.015

738 Lucchitta, B. K. (1979). Landslides in Valles Marineris, Mars. *Journal of Geophysical Research: Solid Earth*,
739 *84*(B14), 8097–8113.

740 Malin, M. C. [Michael C.], Bell, J. F., Cantor, B. A., Caplinger, M. A., Calvin, W. M., Clancy, R. T. [R. Todd], . . .
741 James, P. B. (2007). Context camera investigation on board the Mars Reconnaissance Orbiter. *Journal of*
742 *Geophysical Research: Solid Earth*, *112*(E5).

743 Malin, M. C. [Michael C.], & Edgett, K. S. (2003). Evidence for persistent flow and aqueous sedimentation on early
744 Mars. *Science (New York, N.Y.)*, *302*(5652), 1931–1934. https://doi.org/10.1126/science.1090544

745 Martin, W., Baross, J., Kelley, D., & Russell, M. J. (2008). Hydrothermal vents and the origin of life. *Nature*
746 *Reviews Microbiology*, *6*, 805 EP -. https://doi.org/10.1038/nrmicro1991

747 McEwen, A. S., Eliason, E. M., Bergstrom, J. W., Bridges, N. T., Hansen, C. J., Delamere, W. A., . . . Keszthelyi, L.
748 (2007). Mars reconnaissance orbiter's high resolution imaging science experiment (HiRISE). *Journal of*
749 *Geophysical Research: Solid Earth*, *112*(E5).

750 McNeill, L. C., & Collier, R.E.L. [R.E.Ll.] (2004). Uplift and slip rates of the eastern Eliki fault segment, Gulf of
751 Corinth, Greece, inferred from Holocene and Pleistocene terraces. *Journal of the Geological Society*, *161*(1), 81–
752 92. https://doi.org/10.1144/0016-764903-029

753 Mège, D. [Daniel], & Masson, P. [Philippe] (1996). Amounts of crustal stretching in Valles Marineris, Mars.
754 *Planetary and Space Science*, *44*(8), 749–781.

755 Metz, J., Grotzinger, J., Okubo, C., & Milliken, R. [Ralph] (2010). Thin-skinned deformation of sedimentary rocks
756 in Valles Marineris, Mars. *Journal of Geophysical Research: Solid Earth*, *115*(E11).

757 Metz, J. M., Grotzinger, J. P., Mohrig, D., Milliken, R. [Ralph], Prather, B., Pirmez, C., . . . Weitz, C. M. (2009).
758 Sublacustrine depositional fans in southwest Melas Chasma. *Journal of Geophysical Research: Planets*,
759 *114*(E10), n/a-n/a. https://doi.org/10.1029/2009JE003365

760 Murchie, S. [Scott], Arvidson, R., Bedini, P., Beisser, K., Bibring, J.-P., Bishop, J., . . . Clancy, R. T. [R. T.] (2007).
761 Compact reconnaissance imaging spectrometer for Mars (CRISM) on Mars reconnaissance orbiter (MRO).
762 *Journal of Geophysical Research: Solid Earth*, *112*(E5).

763 Ori, G. G. (1989). Geologic history of the extensional basin of the Gulf of Corinth (?Miocene-Pleistocene), Greece.
764 *Geology*, *17*(10), 918. https://doi.org/10.1130/0091-7613(1989)017<0918:GHOTEB>2.3.CO;2

765 Parker, T. J., Gorsline, D. S., Saunders, R. S., Pieri, D. C., & Schneeberger, D. M. (1993). Coastal geomorphology
766 of the Martian northern plains. *Journal of Geophysical Research: Solid Earth*, *98*(E6), 11061–11078.

767 Parker, T. J., Saunders, R. S., & Schneeberger, D. M. (1989). Transitional morphology in west Deuteronilus
768 Mensae, Mars: Implications for modification of the lowland/upland boundary. *Icarus*, *82*(1), 111–145.

769 Pelkey, S. M., Mustard, J. F. [J. F.], Murchie, S. [S.], Clancy, R. T. [R. T.], Wolff, M., Smith, M., . . . Poulet, F. [F.]
770 (2007). CRISM multispectral summary products: Parameterizing mineral diversity on Mars from reflectance.
771 *Journal of Geophysical Research: Solid Earth*, *112*(E8).

772 Peulvast, J. P., & Masson, P. L. (1993). Melas Chasma: Morphology and tectonic patterns. *Earth, Moon, and*
773 *Planets*, *61*(3), 219–248.

774 Pondrelli, M., Rossi, A. P., Marinangeli, L., Hauber, E. [Ernst], Gwinner, K., Baliva, A., & Di Lorenzo, S. (2008).
775 Evolution and depositional environments of the Eberswalde fan delta, Mars. *Icarus*, *197*(2), 429–451.

776 Quantin, C. [C.], Allemand, P., Mangold, N. [N.], Dromart, G. [G.], & Delacourt, C. (2005). Fluvial and lacustrine
777 activity on layered deposits in Melas Chasma, Valles Marineris, Mars. *Journal of Geophysical Research: Solid*
778 *Earth*, *110*(E12).

779 Quantin, C. [C.], Gendrin, A. [A.], Mangold, N. [N.], Bibring, J. P., Poulet, F. [F.], & Allemand, P. (2005a). Fluvial
780 and lacustrine activity on layered deposits in Melas Chasma, Valles Marineris, Mars. *Journal of Geophysical*
781 *Research*, *110*(E12), 1780. https://doi.org/10.1029/2005JE002440

782 Roberts, S., & Jackson, J. (1991). Active normal faulting in central Greece: An overview. *Geological Society,*
783 *London, Special Publications*, *56*(1), 125–142.

784 Rohais, S., Eschard, R., & Guillocheau, F. (2008). Depositional model and stratigraphic architecture of rift climax
785 Gilbert-type fan deltas (Gulf of Corinth, Greece). *Sedimentary Geology*, *210*(3), 132–145.

786 Schon, S. C., Head, J. W., & Fassett, C. I. (2012). An overfilled lacustrine system and progradational delta in Jezero
787 crater, Mars: Implications for Noachian climate. *Planetary and Space Science*, *67*(1), 28–45.

Seidel, M., Seidel, E., & Stöckhert, B. (2007). Tectono-sedimentary evolution of lower to middle Miocene half-graben basins related to an extensional detachment fault (western Crete, Greece). *Terra Nova*, *19*(1), 39–47. https://doi.org/10.1111/j.1365-3121.2006.00707.x

Ślączka, A., Renda, P., Cieszkowski, M., Golonka, J., & Nigro, F. (2012). Sedimentary basins evolution and olistoliths formation: The case of Carpathian and Sicilian regions. *Tectonophysics*, *568-569*, 306–319. https://doi.org/10.1016/j.tecto.2012.03.018

Stack, K. M. [Kathryn M.], Grotzinger, J. P., Lamb, M. P., Gupta, S. [Sanjeev], Rubin, D. M. [David M.], Kah, L. C., . . . Aileen Yingst, R. (2019). Evidence for plunging river plume deposits in the Pahrump Hills member of the Murray formation, Gale crater, Mars. *Sedimentology*, *66*(5), 1768–1802. https://doi.org/10.1111/sed.12558

Van Wagoner, J. C., Posamentier, H. W., Mitchum, R. M.J., Vail, P. R., Sarg, J. F., Loutit, T. S., & Hardenbol, J. (1988). An overview of the fundamentals of sequence stratigraphy and key definitions.

Vetterlein, J., & Roberts, G. P. (2010). Structural evolution of the Northern Cerberus Fossae graben system, Elysium Planitia, Mars. *Journal of Structural Geology*, *32*(4), 394–406. https://doi.org/10.1016/j.jsg.2009.11.004

Witbeck, N. E., Tanaka, K. L., & Scott, D. H. (1991). *Geologic map of the Valles Marineris region, Mars* (IMAP No. 2010).